Oil Shale, 2017, Vol. 34, No. 3, pp. 232–249
doi: https//doi.org/10.3176/oil.2017.3.03
ISSN 0208-189X

SIMULATION INVESTIGATION OF SINGLE OIL SHALE PARTICLES DRYING IN SUPERHEATED STEAM AND EXPERIMENTAL VALIDATION

LIANGZHI XIA[(a)*], HONGCHUN ZHANG[(a)], JUN HE[(a)], YIBIN YAO[(b)], CAIYUAN YU[(b)]

[(a)] School of Chemical Machinery & Safety, Dalian University of Technology, Dalian 116024, China
[(b)] School of Chemical Engineering, Dalian University of Technology, Dalian 116024, China

Abstract. *Oil shale is an important unconventional energy and has enormous reserves in the world. However, the high moisture content reduces the efficiency of oil production in the pyrolysis process. In this paper, experimental and numerical studies were conducted on the drying performance of single Liu Shu River oil shale particles in superheated steam. A 3-D model was developed to simulate the heat and mass transfer process inside the particle, taking into account its property of anisotropy transfer. Generally, it is concluded that the moisture removal rate increases as the steam temperature increases, while increasing the particle size decreases the moisture removal rate. In the whole drying process, the decreasing drying rate period was longer than the constant drying rate period. The anisotropy had an influence on moisture transfer rather than heat transfer process. The moisture content profiles and temperature fields inside the particle were determined at selected times. Several experiments were carried out under the conditions of different temperatures (463–483 K) and particle sizes (5–9 mm). It was found that the developed model predictions agreed well with the experimental data. It is significant to get the microscopic parameters for the investigation of oil shale drying in superheated steam fluidized bed.*

Keywords: *oil shale particle drying, superheated steam, heat and mass transfer, anisotropy*.

1. Introduction

Crude oil, a limited non-renewable hydrocarbon resource, cannot continue to meet the ongoing and increasing demands of mankind. Oil shale is globally recognized as the most potential replacement of unconventional hydrocarbon

* Corresponding author: e-mail *xialiangzhi0411@163.com*

resources. The reserves of oil shale are estimated at about 500 billion tons, which are widespread in the United States, Russia, China and many other countries [1]. The annual production of shale oil in China may reach 0.78 million tons [2]. However, porous oil shale, densely inside the wool stoma, easily absorbs water. In general, the moisture content of Chinese oil shale is as high as 10–30% (dry basis), but in some areas, such as Maoming and Liu Shu River, it is even higher than 30% (dry basis). In the pyrolysis process, the high moisture content will cause the particle break easily, which results in deteriorating the quality of shale oil and increasing the cost of energy consumption as well as equipment maintenance. Therefore, it is significant to efficiently pre-dry wet oil shale particles [3]. In the past several decades, many studies have been conducted on the drying efficiency of superheat steam [4, 5]. Also, the superheated steam fluidized bed drying (SSFBD) has found wide application, e.g., in the food, low-rank coal and lignite industries [6–9]. Certainly, the drying mechanism of a single particle is the theoretical basis of SSFBD. Some researchers [10, 11] have modeled the steam drying process for porous oil shale particles by obeying the conservation laws.

Based on an assumption about the receding particle core, researchers [12–14] developed a model of drying a single lignite particle. It is necessary to predict and analyze the drying performance of porous ceramic particles. However, the mathematical model of oil shale particle drying cannot always accurately describe the drying mechanism. Some investigators [15–17] explained the drying mechanism by the usual boundary layer approximation which can be described by solving the governing equations during water evaporation from the particle surface.

In this context, the main objective was to develop a mathematical model employing the COMSOL Multiphysics for investigating three main drying periods in the single oil shale particle drying process: the initial condensation-evaporation period, the constant rate drying period and the decreasing rate drying period. Further, the coefficient of moisture diffusion as a function of temperature and moisture content was determined. The anisotropy of effective diffusion, permeability and thermal conductivity of moisture in different directions was determined as well [18, 19]. The experiments were carried out under atmospheric pressure at different temperatures (463–483 K). By modeling, the possible hygroscopicity, as well as formation of shrinks and cracks during the drying process were ignored. It was found that the effective diffusivity of moisture was the critical parameter in modeling SSFBD during the decreasing drying rate stage [20–22].

2. Numerical modeling

A 3-D model was developed to decribe the heat and mass transfer process of a single oil shale particle in superheated steam. In the present work, the

model of effective diffusivity includes the Darcy law of liquid moisture, moisture diffusion in the vapor phase, and diffusion of bound moisture.

2.1. Governing equations

For a single oil shale particle the developed 3-D model is considered as an anisotropic medium whose effective diffusivity in different directions is different.

In the study, the following assumptions are made:

(1) The inner temperature at a given location is shared by all phases at any time.
(2) Particle deformation in the drying process is ignored.
(3) The oil shale particle is in local thermodynamic equilibrium.
(4) Radiation heat transport under given condition is ignored.

In the initial condensation-evaporation period, the condensation temporarily occurs on the particle surface, and then the condensed water evaporates into the superheated steam when pure steam is in contact with the particle surface of relatively low temperature. Heat is transferred from the particle surface to the interior of particle by convection and condensation.

The energy balance for the non-isothermal spherical particle can be written as [23]:

$$(\rho_{eff} C_{p,eff}) \frac{\partial T}{\partial \tau} = \frac{\partial T}{\partial x}\left(\lambda_{eff}^{x} \frac{\partial T}{\partial x} \right) + \frac{\partial T}{\partial y}\left(\lambda_{eff}^{y} \frac{\partial T}{\partial y} \right) + \frac{\partial T}{\partial z}\left(\lambda_{eff}^{z} \frac{\partial T}{\partial z} \right), \tag{1}$$

where λ_{eff}^{x} is the effective thermal conductivity vertical to the bedding plane direction; λ_{eff}^{y} and λ_{eff}^{z} are the effective thermal conductivities parallel to the bedding plane direction; T is the particle temperature.

The wet oil shale particle can be assumed as a spherical droplet. The rate of evaporation or condensation per unit droplet surface area was governed by the modified Hertz-Knudsen equation:

$$-\rho_w \frac{dr}{dt} = \sqrt{\frac{M_w}{2\pi \mathrm{R}_g}} \left[\frac{P_{sat}(T)}{\sqrt{T}} - \frac{P_{atm}}{\sqrt{T_g}} \right], \tag{2}$$

where r is the radius of the liquid water boundary inside particle; $\mathrm{R_g}$ is the universal gas constant.

In the constant and decreasing drying rate periods, the moisture transfer inside the particle is expressed in the same form as the diffusion equation:

$$\frac{\partial M}{\partial \tau} = \frac{\partial M}{\partial x}\left(D_{eff}^{x} \frac{\partial M}{\partial x} \right) + \frac{\partial M}{\partial y}\left(D_{eff}^{y} \frac{\partial M}{\partial y} \right) + \frac{\partial M}{\partial z}\left(D_{eff}^{z} \frac{\partial M}{\partial z} \right), \tag{3}$$

where λ_{eff}^{x} is the effective diffusivity of moisture vertical to the bedding plane direction; λ_{eff}^{y} and λ_{eff}^{z} are the effective diffusivities of moisture parallel to the bedding plane direction.

Apparently, the predicted temperature field in the decreasing drying rate period can be used as the initial temperature field. The model of internal heat conduction can be described by Equation (1).

2.2. Boundary determination of superheated steam drying

During the first drying period, the condensation-evaporation phenomenon occurs at the boundary, bringing and taking away heat, respectively. According to the balance of heat flux, it can be described by:

$$-\lambda_{eff}^{x}\frac{\partial T}{\partial x}-\lambda_{eff}^{y}\frac{\partial T}{\partial y}-\lambda_{eff}^{z}\frac{\partial T}{\partial z}=h_T(T_\infty-T)+\rho_w\Delta H_{vap}\frac{dr}{dt}, \tag{4}$$

where h_T is the heat transfer coefficient; ΔH_{vap} is the latent heat of evaporation.

During the next drying period, in the case of pure superheated steam as the drying medium, there is no convective transport of vapor due to the concentration gradient from the particle surface to the surrounding. The external mass transfer must be taken into consideration [24]:

$$-D_{eff}^{x}\rho_l\frac{\partial M}{\partial x}-D_{eff}^{y}\rho_l\frac{\partial M}{\partial y}-D_{eff}^{z}\rho_l\frac{\partial M}{\partial z}=F_{\max}=\frac{h_T(T-T^*)}{\Delta H_{vap}}, \tag{5}$$

where T^* can be computed from Equation (8).

The energy conservation equation at the boundary is expressed by:

$$-\lambda_{eff}^{x}\frac{\partial T}{\partial x}-\lambda_{eff}^{y}\frac{\partial T}{\partial y}-\lambda_{eff}^{z}\frac{\partial T}{\partial z}=h_T(T_\infty-T)-F_m\Delta H_{vap}. \tag{6}$$

For the mass conservation equation, the boundary condition at the drying surface is determined by the local vapor pressure and the external pressure. The local vapor pressure is equal to its equilibrium pressure [25]:

$$P_{v,\mathrm{eq}}=a_w(X,T)P_{\mathrm{sat}}\left(T\right)=P_\infty, \tag{7}$$

where the saturation pressure of the vapor phase [26] is obtained by Equation (8), according to the Arrhenius law which considers the activation energy E_a as an adjustable parameter:

$$P_{\mathrm{sat}}\left(T\right)=610\exp\left[17.269\times(T_\infty-273)/(237.5+T_\infty-273)\right]. \tag{8}$$

In the present work, it is assumed that the activation energy is constant. The coefficient D_0 increases with decreasing particle diameter [27, 28]. It is difficult to give a physical explanation for the moisture diffusion inside the particle following a model in the Knudsen diffusion when the particle diameter increases [29]. Also, it is necessary to understand the fracture mechanics inside the oil shale particle to have a good complement to

developing the mass transfer model. The moisture diffusion in the particle can be expressed as follows [30]:

$$D_{eff} = D_0 \exp\left(-\frac{E_a}{\mathrm{R}_g T_a}\right)\exp(-(AT_a + B)M). \tag{9}$$

The related parameters are given in Table 1.

Table 1. The effective diffusion coefficient

Particle number	Particle size, mm	E_a, kJ/mol	D_0, m^2/s	A, K^{-1}	B
1, 4	9	89	1×10^{-6}	0.05	0.2
2, 5	7	89	6×10^{-7}	0.05	0.2
3, 6	5	89	4×10^{-7}	0.05	0.2

2.3. Numerical solution

The main drying parameters are given in Table 2. The finite element software COMSOL Multiphysics is used to solve the equations to study the drying process of a single oil shale particle in superheated steam. From Table 2 it can be seen that the mass transfer coefficients for the Liu Shu River oil shale in two directions are different.

Table 2. Main drying parameters

Parameter	Parallel to the bedding plane direction	Vertical to the bedding plane direction
Moisture diffusion, $m^2 \cdot s^{-1}$	D_{eff}	$(1/5) \times D_{eff}$
Thermal conductivity, $W \cdot m^{-1} \cdot K^{-1}$	$\lambda_p = 0.4474$	$\lambda_V = 0.4128$
Initial temperature, K	$T_0 = 298$	
Porosity	$\varepsilon = 0.3$	
Oil shale density, $kg \cdot m^{-3}$	$\rho_P = 1897 - 865 \times X$	
Oil shale specific heat, J/(kg·K)	$C_P = 842 + 3.97 \times T - 2.2371 \times 10^{-2} \times T^2 + 1.101 \times 10^{-4} \times T^3$	
Latent heat, J/kg	$\Delta H_{vap} = 3168 - 2.4364 \times T$	
Heat transfer coefficient, $W \cdot m^{-2} \cdot K^{-1}$	$h_T = Nu\lambda_g / d$	
Nusselt number	$Nu = 2 + 0.66\,\mathrm{Re}^{0.52}\,\mathrm{Pr}^{0.33}$	
Time step, s	0.1	

3. Experimental section

The oil shale sample for the study was obtained from the Liu Shu River area, China. Table 3 presents the initial moisture content of oil shale and the experimental drying conditions. The sample was manufactured into spherical particles of different sizes. The procedure was repeated at least three times to obtain a representative average. The experiments were carried out to demonstrate the effect of steam temperature and particle size on the drying

characteristics under certain conditions. A schematic diagram of the experimental system is shown in Figure 1. A self-designed superheated steam generator equipped with process variables controllers was employed. The constant mass flow rate (m_w = 0.000501 kg/s) was obtained by adjusting the heating power of the steam generator through the voltage regulator. Steam pressure was maintained at atmospheric pressure. The steam generated from the heating jacket was heated to a specified temperature, and then became superheated steam. The oil shale particle hanging in a thin wire was dried by the superheated steam flowing through the drying tube. The exhaust gas was discharged from the outlet. The real-time electronic balance recorded the weight of a single particle in the drying process every 10 s.

Table 3. Experimental drying conditions

Temperature of steam, K	Particle number	Particle diameter, mm	Initial moisture content M_0, % (dry basis)
463	1	9	23.51
463	2	7	33.42
463	3	5	25.19
483	4	9	26.67
483	5	75	22.23
483	6		23.23

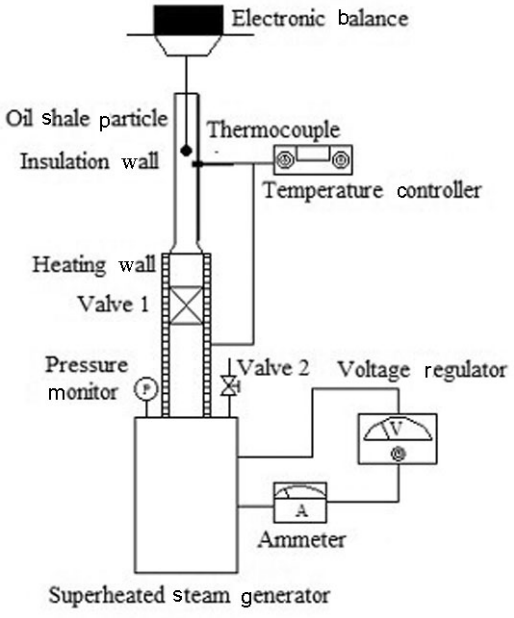

Fig. 1. Schematic diagram of the experimental system.

4. Results and discussion

4.1. Numerical identification of the effective diffusion coefficient of moisture

The effective diffusion coefficient of moisture is described by the mathematical model related to moisture content and particle temperature. It was indicated that there was a certain relationship between void fraction and anisotropic moisture diffusion by comparing theory with experiments [31, 32]. Figure 2a–b plots the effective moisture diffusivity variations in the

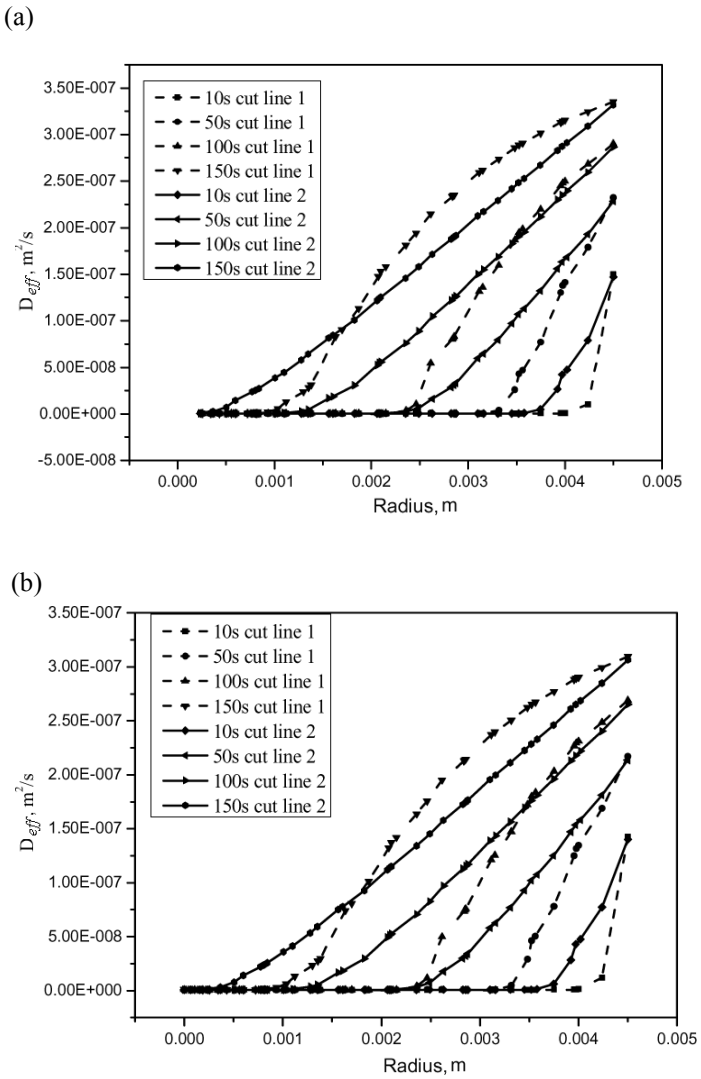

Fig. 2. Variation of effective moisture diffusivity in the radial direction at different steam temperatures: (a) T = 483 K; (b) T = 463 K.

radial direction in the 9 mm particle at a steam temperature of T = 483 K and T = 463 K, respectively. (Cut line 1 is vertical to the bedding plane direction while Cut line 2 is parallel to the bedding plane direction). It can be observed from Figure 2 that the effective diffusivity increases as the moisture content decreases (time increase) and temperature increases. It may be attributed to vapor generation at a higher rate. Figure 3 shows that the particle diameter greatly affects the rate of moisture transfer. It can be explained by the fact that a smaller particle has a larger specific surface area and a higher rate of moisture transfer. The moisture is transferred along the shorter path to the surface in a shorter time.

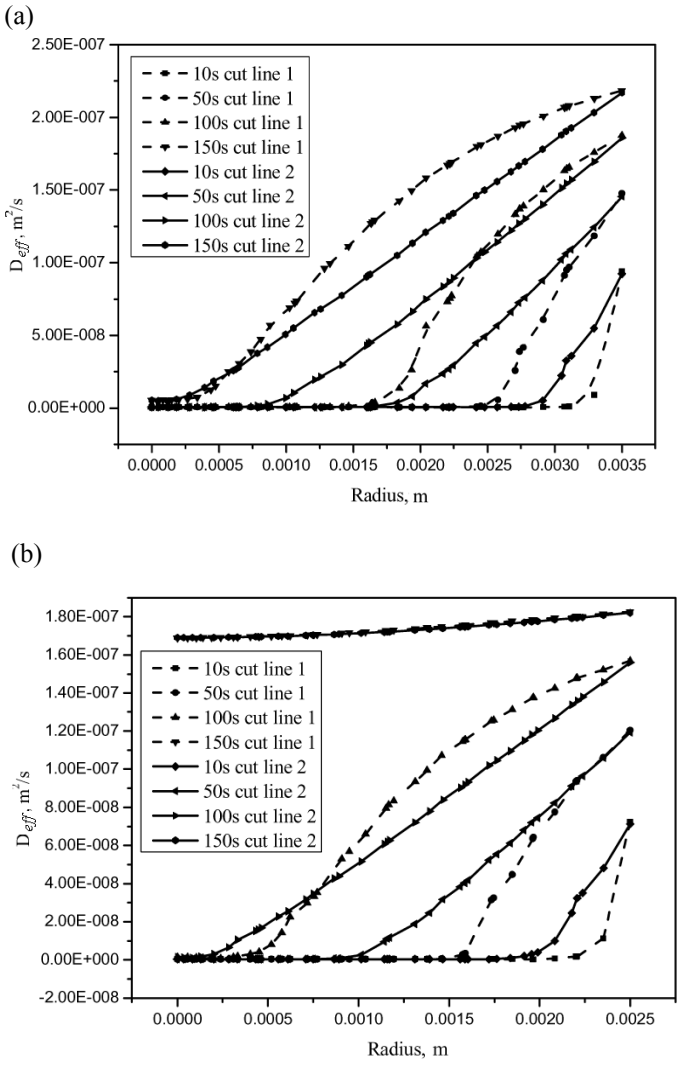

Fig. 3. Variation of effective moisture diffusivity in the radial direction for different particle sizes at a steam temperature of 463 K: (a) d = 7 mm; (b) d = 5 mm.

Figure 4 shows that the anisotropy has an obvious influence on moisture transfer, which increases first and then decreases because the particle moisture content in the final stage of drying is too low. Figure 5 plots particle moisture profiles at 10 s, 50 s, 100 s and 150 s at a steam temperature of 463 K and particle size of 7 mm. The blue and red interfaces are the dry-wet interfaces which are observed in many experiments. It is indicated that the developed drying model of single particles can be adapted to the oil shale drying process.

Figure 6 shows the change in particle temperature in the radial direction at a steam temperature of 463 K and particle size of 7 mm at 50 s. It can be seen that particle temperature has no anisotropic property. Figure 7 plots particle temperature profiles at different times like 10 s, 50 s, 100 s and 150 s under the same conditions. The temperature of the oil shale particle changes quickly due to the occurrence of the condensation reaction in the initial drying stage. A lot of heat is generated when the vapor phase transition takes place. The particle temperature exhibits a uniform upward trend until the moisture content of the particles reaches the equilibrium.

As can be seen from Figures 8–10, there takes place a short steam condensation process when the particle temperature in the initial, preheating stage quickly rises. But the drying model matches the variation of moisture content well because the steam temperature drops below the temperature of dew point by contacting particles with relatively low temperature, and the particle temperature rises quickly by acquiring a lot of heat due to the phase transition. The moisture contents obtained by modeling agree well with the experimental data. It is verified that the mathematical model can describe the drying performance of a single porous oil shale particle. Figure 8 shows that there is a wide discrepancy between the experiment and simulation with

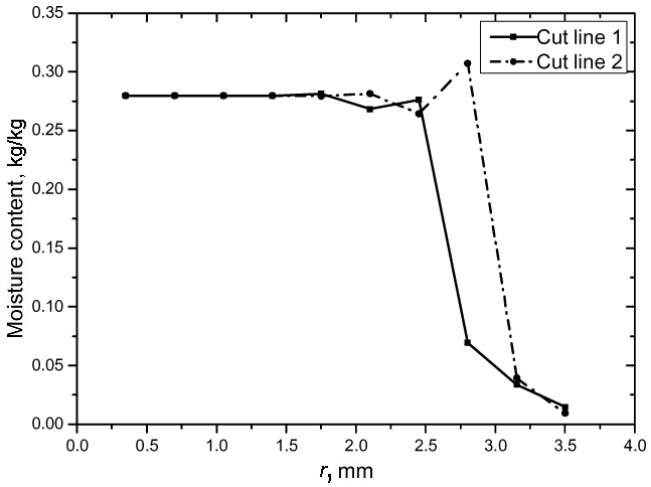

Fig. 4. Variation of particle moisture content in the radial direction at a steam temperature of 463 K and particle size of 7 mm at 50 s.

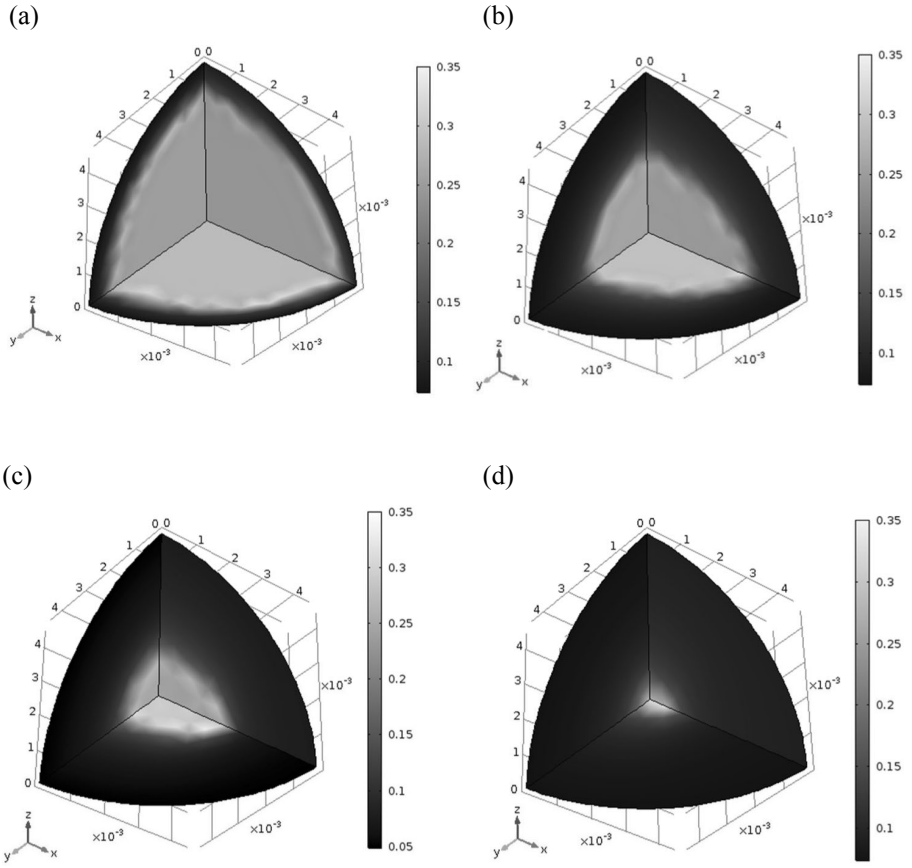

Fig. 5. Particle moisture profiles at different times: (a) t = 10 s; (b) t = 50 s; (c) t = 100 s; (d) t = 150 s.

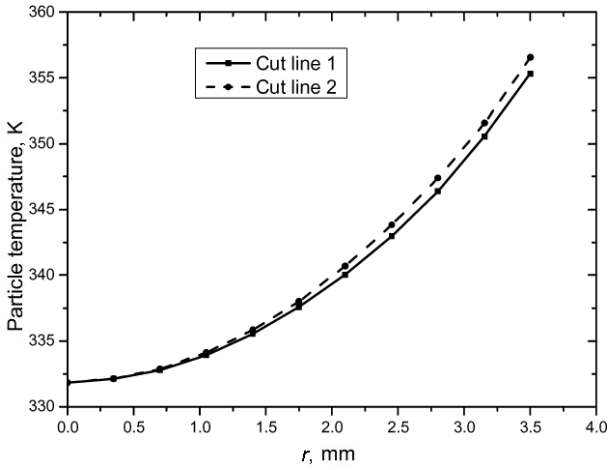

Fig. 6. Variation of particle temperature in the radial direction at 50 s.

a large deviation at 250 s. It may be caused by a higher differential temperature stress and moisture difference between the particle surface and the interior of the larger particle. At the same time, the high drying rate leads to a short constant rate drying stage occurring at 373 K at atmospheric pressure. From Figure 11 it is seen that the drying rate increases as the size of a particle with a larger specific surface area decreases. Decreasing particle size is helpful to improve the drying rate in the drying process.

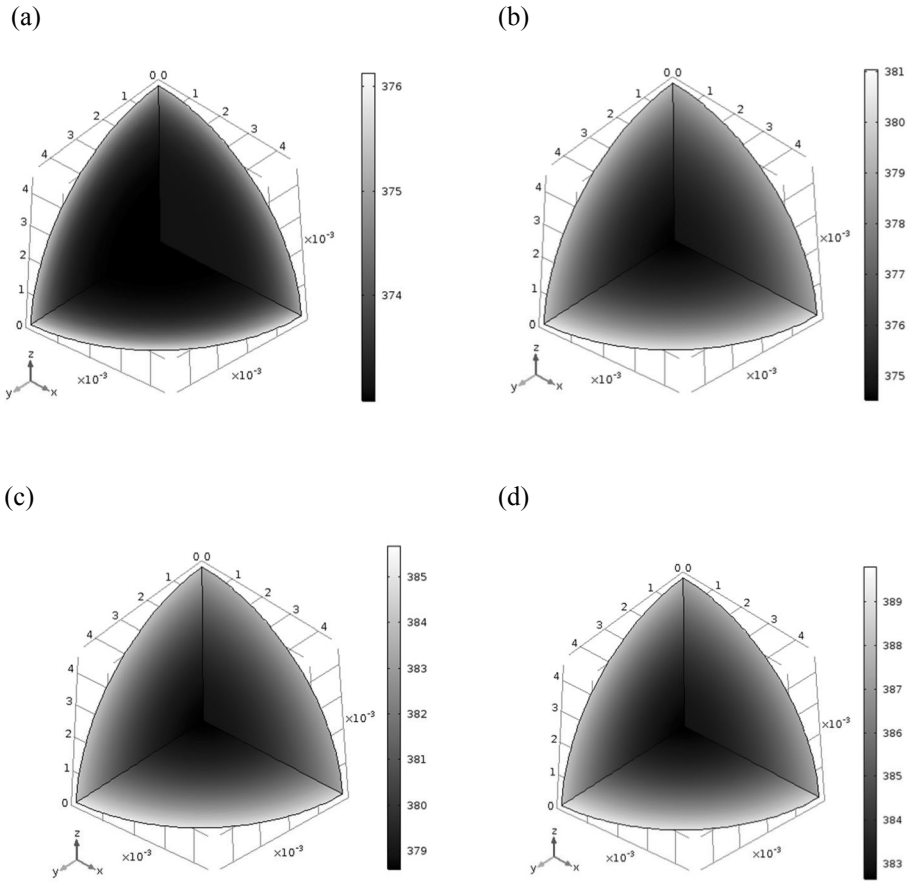

Fig. 7. Particle temperature distribution at T = 483 K and different times: (a) t = 10 s; (b) t = 50 s; (c) t = 100 s; (d) t = 150 s.

(a)

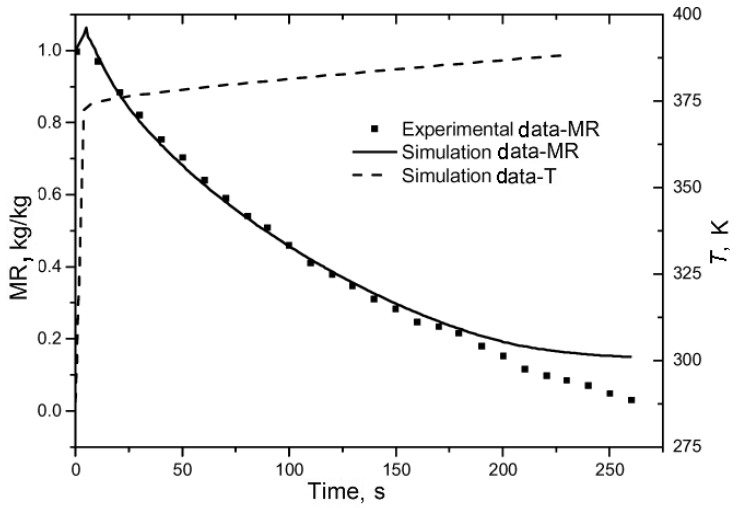

(b)

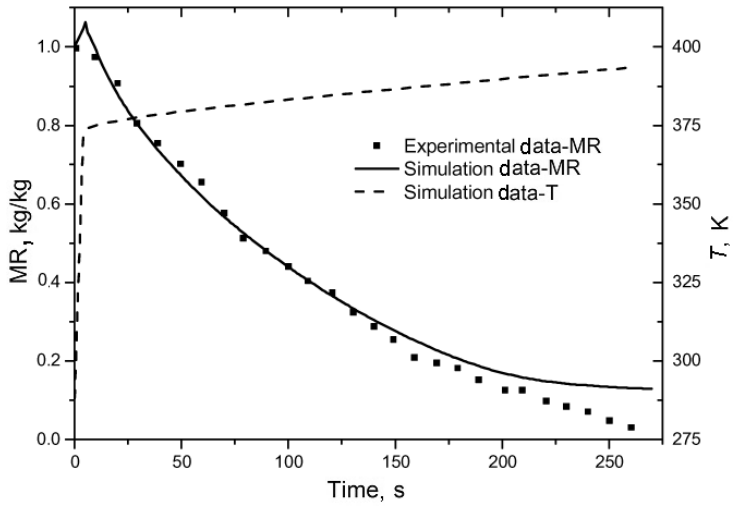

Fig. 8. Average moisture content and temperature (0, 0, 4.5 mm) profiles within a particle of 9 mm at different steam temperatures: (a) $T = 463$ K; (b) $T = 483$ K. (The abbreviation used: MR – moisture rate.)

(a)

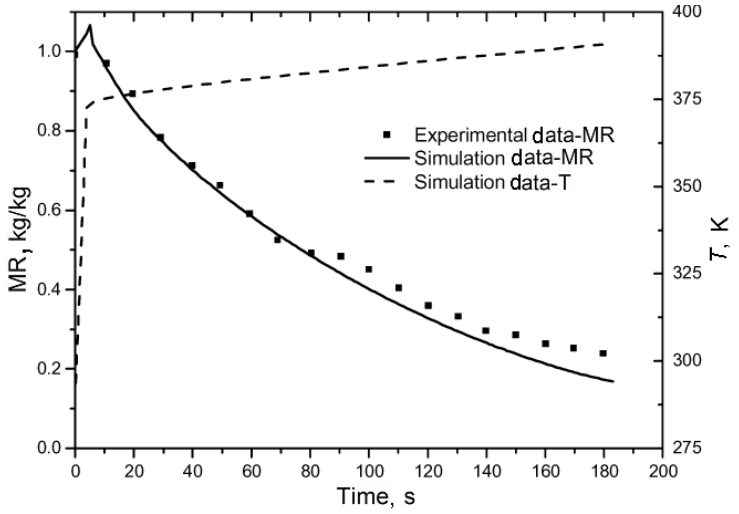

(b)

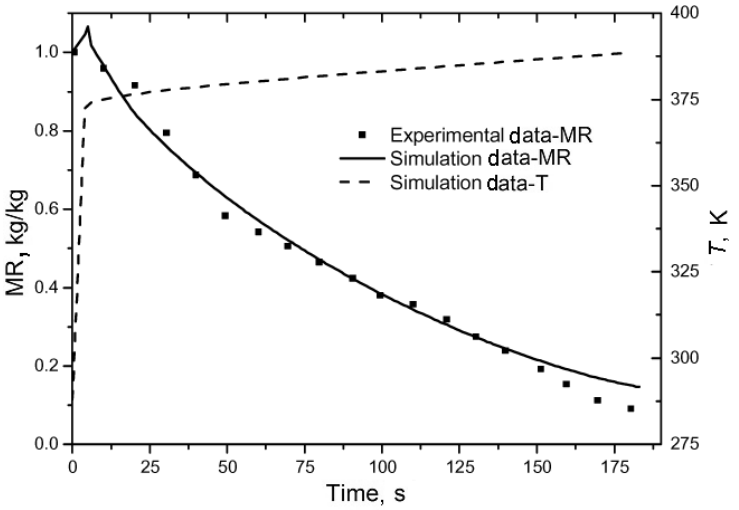

Fig. 9. Average moisture fraction and temperature (0, 0, 3.5 mm) profiles within a particle of 7 mm at different steam temperatures: (a) $T = 463$ K; (b) $T = 483$ K. (The abbreviation used: MR – moisture rate.)

(a)

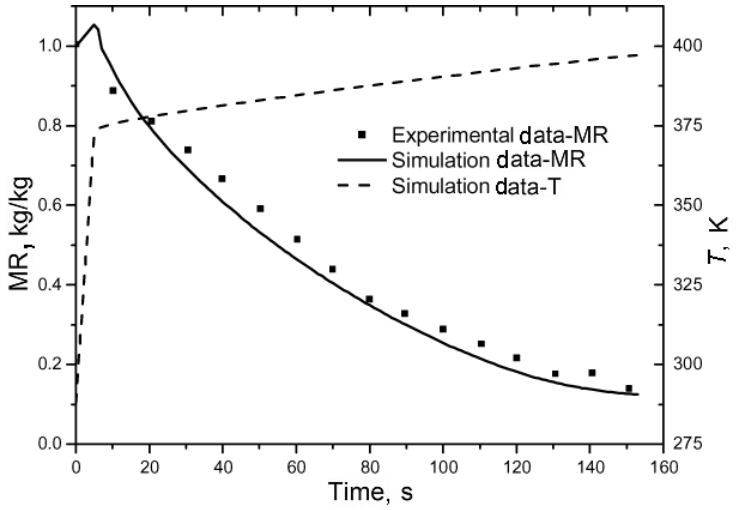

(b)

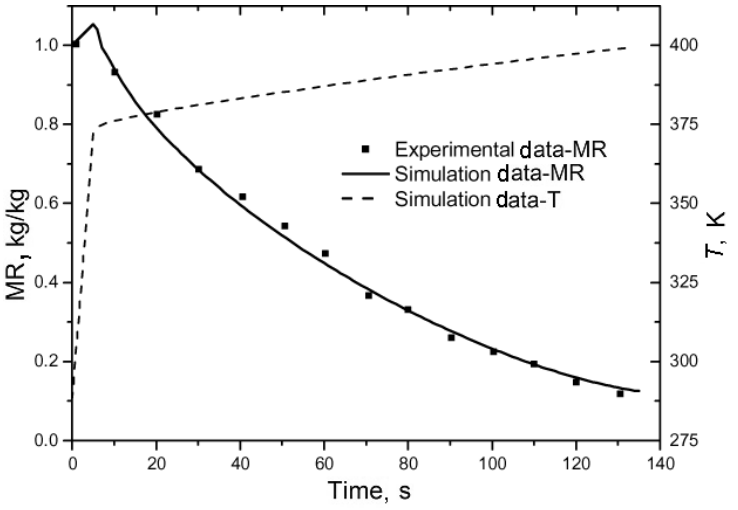

Fig. 10. Average moisture fraction and temperature (0, 0, 2.5 mm) profiles within a particle of 5 mm at different steam temperatures: (a) T = 463 K; (b) T = 483 K. (The abbreviation used: MR – moisture rate.)

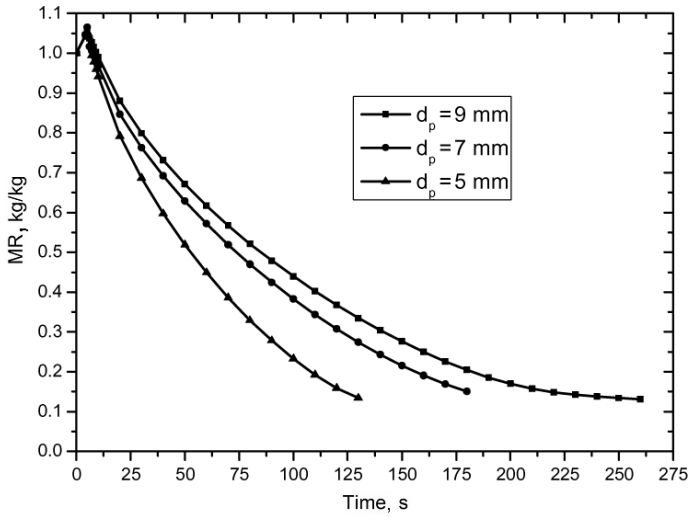

Fig. 11. The effect of particle size on moisture content at a steam temperature of 483 K. (The abbreviation used: MR – moisture rate.)

5. Conclusions

A drying model was developed to simulate the drying behavior of single oil shale particles in superheated steam. The precise temperature and moisture fields could be predicted. The experiments were carried out at different steam temperatures and with particles of different sizes.

The main conclusions drawn are as follows:

1. The anisotropy influences moisture transfer rather than heat transfer.
2. The drying time is reduced by increasing the steam temperature and decreasing the particle size.
3. In the whole drying process, there is neither distinct condensation process nor constant drying rate period. In addition, the oil shale drying is characterized by a long decreasing drying rate period.
4. The numerical modeling results agreed well with the experimental data. It is verified that the mathematical model can describe the drying performance inside the oil shale particle.
5. It is meaningful to determine the effective moisture diffusivity which is a critical parameter in modeling superheated steam fluidized bed drying in the third stage of the process.

Nomenclature

Cp = specific heat, J/(kg·K)
D = diffusivity, m^2/s
d_p = particle diameter, mm
M_w = molecular weight of water, kg/mol

P = pressure, Pa
R = universal gas constant, J/(K·mol)
T = temperature, K
m = constant mass flow rate, kg/s
M = dry-basis moisture content, kg/kg
ΔH_{vap} = latent heat of vaporization, J/kg
E_a = activation energy, kJ/mol
F = mass flux, $kg \cdot s^{-1} \cdot m^{-2}$
r = radius of the liquid water boundary inside particle, mm
X = wet-basis moisture content, kg/kg

Greek letters
λ = thermal conductivity, $W \cdot m^{-1} \cdot K^{-1}$
ε = porosity
μ = dynamic viscosity, $kg \cdot m^{-1} \cdot s^{-1}$
ρ = density, $kg \cdot m^{-3}$
τ = drying time, s

Subscripts and superscripts
0 = standard state
eff = effective
g = gas mixture
w = liquid water
p = solid particle
sat = saturated state
v = water vapor
center = center of particles
sur = surface of particles
∞ = ambient

REFERENCES

1. Hilger, J. Combined utilization of oil shale energy and oil shale minerals within the production of cement and other hydraulic binders. *Oil Shale*, 2003, **20**(3S), 347–355.
2. Chen, M., Cheng, Y., Li, W. Exploitation and utilization of oil shale in the coal measure strata of the Haishiwan mine, Yaojie coalfield, China. *Oil Shale*, 2015, **32**(4), 335–355.
3. Golubev, N. Solid oil shale heat carrier technology for oil shale retorting. *Oil Shale*, 2003, **20**(3S), 324–332.
4. Volkov, E., Potapov, O. The optimal process to utilize oil shale in power industry. *Oil Shale*, 2000, **17**(3), 252–260.
5. Van Deventer, H. C., Heijmans, R. M. H. Drying with superheated steam. *Dry. Technol.,* 2001, **19**(8), 2033–2045.
6. Stokie, D., Meng, W. W, Bhattacharya, S. Comparison of superheated steam and air fluidized-bed drying characteristics of Victorian brown coals. *Energ. Fuel.*, 2013, **27**(11), 6598–6606.
7. Rordprapat, W., Nathakaranakule, A., Tia, W. Comparative study of fluidized bed paddy drying using hot air and superheated steam. *J. Food Eng.*, 2005, **71**(1), 28–36.
8. Katalambula, H., Gupta, R. Low-grade coals: a review of some prospective upgrading technologies. *Energ. Fuel.,* 2009, **23**(7), 3392–3405.

9. Chen, Z., Agarwal, P. K., Agnew, J. B. Steam drying of coal. Part 2. Modeling the operation of a fluidized bed drying unit. *Fuel*, 2001, **80**(2), 209–223.
10. Messai, S., Sghaier, J., Lecomte, D., Belghith, A. Drying kinetics of a porous spherical particle and the inversion temperature. *Dry. Technol.,* 2008, **26**(2), 157–167.
11. Suvarnakuta, P., Devahastin, S., Mujumdar, A. S. A mathematical model for low-pressure superheated steam drying of a biomaterial. *Chem. Eng. Process.*, 2007, **46**(7), 675–683.
12. Zhang, K., You, C. Experimental and numerical investigation of convective drying of single coarse lignite particles. *Energ. Fuel.,* 2010, **24**(12), 6428–6436.
13. Chen, Z., Wu, W., Agarwal, P. K. Steam-drying of coal. Part 1. Modeling the behavior of a single particle. *Fuel,* 2000, **79**(8), 961–974.
14. Looi, A. Y., Golonka, K., Rhodes, M. Drying kinetics of single porous particles in superheated steam under pressure. *Chem. Eng. J.,* 2002, **87**(3), 329–338.
15. Volchkov, E. P., Leontiev, A. I., Makarova, S. N. Finding the inversion temperature for water evaporation into an air–steam mixture. *Heat Mass Transfer,* 2007, **50**(11–12), 2101–2106.
16. Debbissi, C., Orfi, J., Nasrallah, S. B. Evaporation of water by free or mixed convection into humid air and superheated steam. *Heat Mass Transfer*, 2003, **46**(24), 4703–4715.
17. Costa, V. A. F., Silva, F. N.D. On the rate of evaporation of water into a stream of dry air, humidified air and superheated steam, and the inversion temperature. *Heat Mass Transfer*, 2003, **46**(19), 3717–3726.
18. Henriksen, U., Hindgaul, C., Qvale, B., Fjellerup, J., Jensen, A. D. Investigation of the anisotropic behavior of wood char particles during gasification. *Energ. Fuel.*, 2006, **20**(5), 2233–2238.
19. Topgaard, D., Söderman, O. Self-diffusion in two-and three-dimensional powders of anisotropic domains: an NMR study of the diffusion of water in cellulose and starch. *J. Phys. Chem-US,* 2002, **106**(46), 11887–11892.
20. Prachayawarakorn, S., Prachayawasin, P., Soponronnarit, S. Heating process of soybean using hot-air and superheated-steam fluidized-bed dryers. *Food Sci. Technol-LEB*, 2006, **39**(7), 770–778.
21. Jang, J., Arastoopour, H. CFD simulation of a pharmaceutical bubbling bed drying process at three different scales. *Powder Technol.*, 2014, **263**, 14–25.
22. Soponronnarit, S., Prachayawarakorn, S., Rordprapat, W., Nathakaranakule, A., Tia, W. A superheated-steam fluidized-bed dryer for parboiled rice: testing of a pilot-scale and mathematical model development. *Dry. Technol.*, 2006, **24**(11), 1457–1467.
23. Sabarez, H. T. Computational modelling of the transport phenomena occurring during convective drying of prunes. *J. Food Eng.,* 2012, **111**(2), 279–288.
24. Messai, S., Sghaier, J., El Ganaoui, M.E, Chrusciel, L., Gabsi, S. Low-pressure superheated steam drying of a porous media. *Dry. Technol.*, 2015, **33**(1), 103–110.
25. Pakowski, Z., Adamski, R., Kokocińska, M., Kwapisz, S. Generalized desorption equilibrium equation of lignite in a wide temperature and moisture content range. *Fuel*, 2011, **90**(11), 3330–3335.
26. Pawlak-Kruczek, H., Plutecki, Z., Michalski, M. Brown coal drying in a fluidized bed applying a low-temperature gaseous medium. *Dry. Technol.*, 2014, **32**(11), 1334–1342.

27. Tütüncü, M. A., Labuza, T. P. Effect of geometry on the effective moisture transfer diffusion coefficient. *J. Food Eng.,* 1996, **30**(3–4), 433–447.
28. Tang, J., Sokhansanj, S. Moisture diffusivity in laird lentil seed components. *T. ASAE*, 1993, **36**(6), 1791–1798.
29. Duffy, B. L., Haynes, B. S. Transport mechanisms in oil shale drying and pyrolysis. *Energ. Fuel.*, 1992, **6**(6), 831–835.
30. Azzouz, S., Guizani, A., Jomaa, W., Belghith, A. Moisture diffusivity and drying kinetic equation of convective drying of grapes. *J. Food Eng.,* 2002, **55**(4), 323–330.
31. Weissberg, H. L. Effective diffusion coefficient in porous media. *J. Appl. Phys.,* 1963, **34**(9), 2636–2639.
32. Kim, J.-H., Ochoa, J. A., Whitaker, S. Diffusion in anisotropic porous media. *Transport Porous Med.*, 1987, **2**(4), 327–356.

Presented by S. Li and V. Oja
Received July 23, 2016